The electrode-electrolyte interface in CO2 reduction and H2 evolution: a multiscale approach

Cecilio de Oliveira Monteiro, M

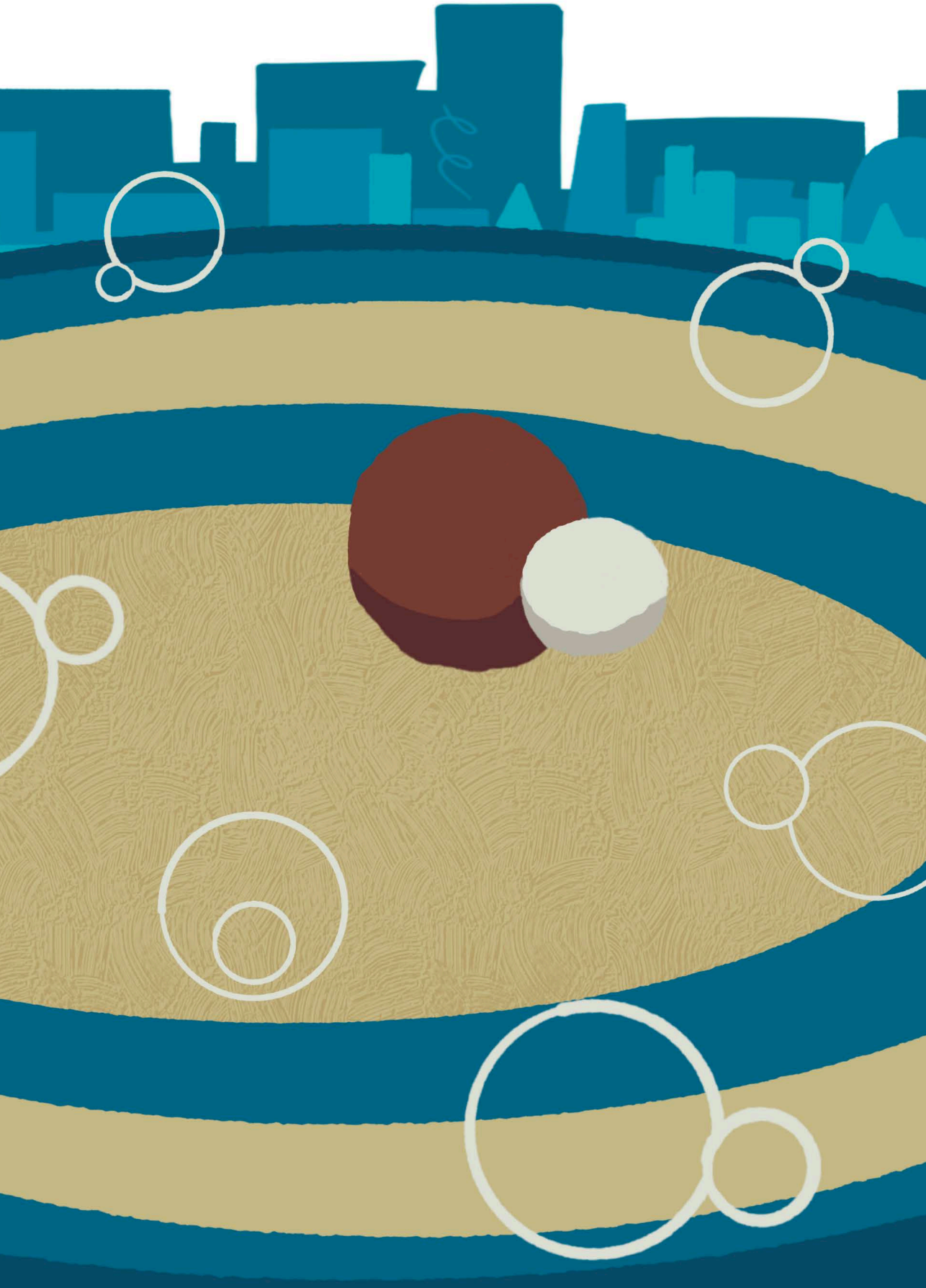

6

Interfacial pH measurements using a Rotating Ring-Disc electrode with a voltammetric pH sensor

This chapter is based on Monteiro, M. C. O., Liu, X., Hagedoorn, B. J. L., Snabilié, D., Koper, M. T. M. *ChemElectroChem*, *8,* DOI: 10.1002/celc.202101223 (2021)

Abstract

Electrochemical reactions in which H^+ or OH^- ions are produced or consumed, affect the pH near the electrode surface. Probing the pH locally is therefore highly desired to understand and model the reaction environment under *operando* conditions. We carried out interfacial pH measurements under mass transport control using a rotating ring-disc electrode (RRDE) coupled with our recently developed voltammetric pH sensor. The interfacial disc pH is detected by functionalizing the gold ring with a hydroxylaminothiophenol (4-HATP)/4-nitrosothiophenol (4-NSTP) redox couple. As protons only have to interact with a monolayer containing the 4-HATP/4-NSTP, the sensitivity and time resolution that can be achieved are superior to potentiometric sensors. We used hydrogen evolution as a model reaction and performed measurements in buffered and unbuffered electrolytes. The effects of the current density, potential, the buffer capacity of the electrolyte and rotation rate on the interfacial pH were investigated. This work shows a reliable and sensitive method for accurately probing the reaction environment under well-defined mass transport conditions, over a wide pH range.

6.1 Introduction

The electrochemical reactions that consume/produce protons or hydroxyl ions can generate a pH gradient between the electrode surface and the bulk of the electrolyte. In general, the value of the local pH developed at the surface is a function of the current drawn, the electrolyte composition, and the mass transport conditions.[1] It has been shown that the (local) electrolyte pH plays a significant role in various reactions, such as hydrogen evolution[2] (HER), CO_2 reduction[3], oxygen evolution[4] and reduction[5], among others. Therefore, it is highly desired to probe the pH gradient near the surface during these electrochemical reactions, with high sensitivity, and with good time and spatial resolution.

In Chapter 2 we review the main techniques available for performing local pH measurements[1], the most frequently used ones being Scanning Electrochemical Microscopy (SECM)[6–8], Scanning Ion Conductance Microscopy (SICM)[9,10], Scanning Ion Selective Electrode (SIET), Rotating Ring-Disc Electrode (RRDE)[11–14], confocal fluorescence scanning microscopy[15], infra-red[16,17] and Raman spectroscopy.[18] Among these, RRDE is the only technique that allows for measurements to be performed under well-defined mass transport conditions, at the expense of the in-plane spatial resolution. Firstly introduced by Albery and Calvo[19–21], pH measurements using RRDE consist of a reaction taking place at the disc electrode and the detection of the proton concentration during the course of this reaction by a pH sensing material at the ring electrode. Due to the electrode geometry and rotation, the flow of species going from the disc to the ring is described by a convective-diffusion equation. This allows the interfacial pH observed at the ring electrode to be directly converted into the pH at the surface of the disc electrode. The advantage is that the detection by the ring electrode does not affect the reactions taking place on the disc electrode. The analytical solution derived by Albery and Calvo[19–21] was recently further developed by Yokoyama et al.[22] by including the autoprotolysis of water in the description, which allows for determining the disc pH more accurately in a wider pH range.

A few works on interfacial pH measurements with RRDE have been reported, however mainly potentiometric pH sensors were employed, the most common being iridium oxide (IrO_x).[11,13,14] The ring electrode is normally modified with an IrO_x film and the pH at the disc is determined based on the Nernstian open circuit potential (OCP) response of the ring. A major drawback of using IrO_x is that the stability and time resolution depend, for example, on the film thickness and pH.[23,24]

Besides IrO_x, certain reactions on bare metal surfaces have also been used to estimate changes in interfacial pH. Figueiredo et al.[12] used shifts in the equilibrium potential of the hydrogen evolution reaction on a Pt ring to estimate the disc pH during ethanol oxidation. Zhang et al. used the CO oxidation reaction on a gold ring to probe the interfacial disc pH during CO_2 reduction to CO on gold.[13] However, it is known that the sensitivity and accuracy of these measurements can be highly compromised by the reaction environment, as both HER and CO oxidation have shown to be affected, i.e. by the cation[25–27], surface structure[28,29] and pH.[30,31] Also, buffering species in the electrolyte are not always taken into account when converting the pH measured at the ring to the interfacial disc pH, which may lead to an overestimation of the local alkalinity. Besides that, based on the analytical description of Yokoyama et al.[22], a small change in pH detected by the ring may correspond to an order of magnitude higher changes of the interfacial disc pH, especially in solutions far from neutral pH. Therefore, a more sensitive pH sensor for RRDE is desired, and in fact necessary, for performing accurate interfacial pH measurements with this technique.

In this Chapter, we have assessed the feasibility of using our recently developed voltammetric pH sensor (Chapter 3) in the RRDE configuration. The sensor consists of a self-assembled monolayer on gold, and in Chapters 3-5 was used for pH measurements in the diffusion layer with SECM.[32,33] The pH response is based on the voltammetry of the hydroxylaminothiophenol (4-HATP)/4-nitrosothiophenol (4-NSTP) redox couple, specifically the Nernstian shift of the oxidation reaction mid-peak potential. We show here that the 4-HATP/4-NSTP voltammetric response is not affected by the electrode rotation, and that this redox couple can be used in a RRDE system. We employed it to probe the interfacial disc pH during hydrogen evolution in buffered and unbuffered electrolytes at mildly acidic pH. With the high sensitivity and time resolution of this voltammetric sensor, we measured the interfacial disc pH during cyclic voltammetry, chronoamperometry and chronopotentiometry experiments, and also determined the rotation rate required to minimize interfacial pH changes in the electrolytes studied. The application of this sensitive and reliable pH sensor for RRDE pH measurements presents an alternative to commonly used potentiometric sensors, and a step forward to more accurately probing the reaction environment under well-defined mass transport conditions.

6.2 Functionalization of the ring electrode

Interfacial pH measurements during hydrogen evolution (HER) using a rotating ring-disc electrode (RRDE) were performed using the electrode assembly schematically represented in Fig. 6.1a. Prior to measurements, the gold ring and disc electrodes are characterized by blank voltammetry, to assure a clean and reproducible surface (see Fig. C.3a in Appendix C). For the pH sensing, the gold ring is modified with a self-assembled monolayer of 4-NTP, which is then electrochemically converted to the 4-HATP/4-NSTP redox couple by cyclic voltammetry, as shown in Fig. 6.1b. The 4-NTP modified gold ring is immersed in the electrolyte under potential control (0.3 V vs. Ag/AgCl) and then a cathodic sweep at 100 mV s^{-1} is performed to partially reduce the monolayer to 4-HATP. The voltammetry of the resulting 4-HATP/4-NSTP redox couple is also shown in Fig. 6.1b recorded at 200 mV s^{-1} (in red), which is the scan rate used during the pH measurements. In principle, even higher scan rates can be used (up to 500 mV s^{-1}), if the process being studied requires better time resolution. Different from our previous work (Chapter 3-5), here the molecule conversion was performed in the same electrolyte as in which HER was carried out. We find that it gives similar results as in the previously used 0.1 M H_2SO_4 if the 60 mV/pH Nernstian shift of the potential window is taken into account. We show here the voltammetry for the conversion in 0.1 M K_2SO_4 at pH = 4 (Fig. 6.1b). In Fig. C.3b in Appendix C, the same is shown in 0.1 KH_2PO_4 and 0.1 M H_2SO_4, for comparison. The molecule conversion has also been successfully performed in, for example, perchlorate and bicarbonate electrolytes, although not shown here.

Before performing the interfacial pH measurements, we have investigated if the rotation of the electrode has any influence on the 4-HATP/4-NSTP response. The ring voltammetry (CV) was constantly recorded while the rotation rate was varied. Results are shown in Fig. 6.1c going from 0 to 2600 rpm. Each data point is the average mid-peak potential (E_{peak}) determined from 10 consecutive cycles together with the standard deviation, and the corresponding CVs are shown in the graph inset. We observe a stable E_{peak} of 0.109 V vs. Ag/AgCl for all rotation rates. There is a slight decrease in the absolute ring current, however this does not affect the peak fitting and extraction of E_{peak}. These results assure that any changes in the ring voltammetry during HER are due to the reaction taking place at the disc, and not affected by the rotation rate or the turbulence of the electrolyte. This is very important, especially when working far from neutral pH. As shown in Fig. 6.1d,

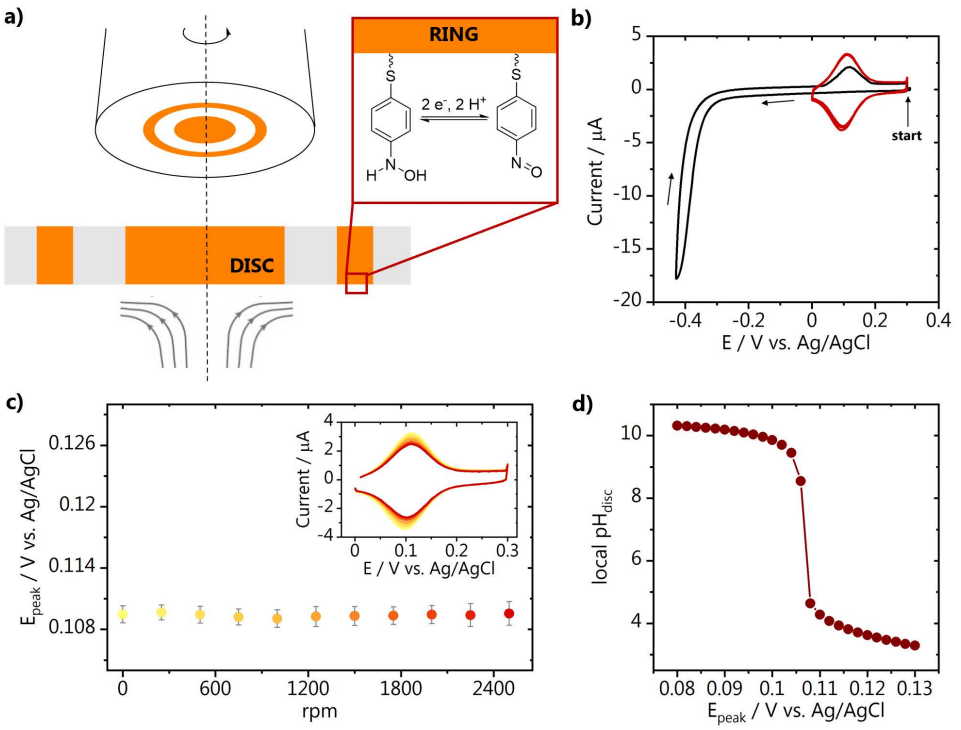

Fig. 6.1. a) Schematic representation of the RRDE with the functionalized ring; **b)** cyclic voltammetry of the 4-NTP to 4-HATP conversion (black, 100 mV s^{-1}) together with a characterization of the 4-HATP/4-NSTP redox couple (red, 200 mV s^{-1}). Both were recorded in 0.1 M K_2SO_4, pH = 4. **c)** Effect of rotation on the pH sensor mid-peak potential, extracted from the voltammograms shown in the inset. **d)** Theoretical relationship between E_{peak} and pH_{disc} using Eq. C.2 for pH_∞ = 4.

considering an unbuffered electrolyte with a bulk pH of 4, a difference of 20 mV in E_{peak} corresponds to a change in pH_{disc} of 7 pH units. The entire E_{peak} range plotted is actually only 50 mV, which corresponds to the detection of a change of less than a unit in the interfacial ring pH. This also indicates how important it is that the pH sensor employed for RRDE measurements is sensitive and stable enough, to measure the interfacial pH accurately. Fig. C.2 in Appendix C shows the theoretical relationships between pH_{Disc} and pH_{Ring} at various pH_∞, comparing Eq. C.2 (Yokoyama) and Eq. C.1 (Albery and Calvo) for an unbuffered electrolyte. The theoretical relationship that can be obtained using the correction we applied for phosphate buffered solutions of different bulk pH is shown in Fig. C.2c. Further experimental details are found in Appendix C.

6.3 Interfacial pH measurements during hydrogen evolution

We employed the modified ring electrode to measure the development of the interfacial pH during a cyclic voltammogram on the gold disc. Hydrogen evolution voltammetry was carried out in phosphate and sulfate electrolyte and the correlation between the current density and the measured interfacial disc pH can be seen in Fig. 6.2a and Fig. 6.2b, respectively. It is important to point out that the conversion from the measured ring pH to the disc pH is done differently for the experiment in unbuffered sulphate electrolyte in comparison to the phosphate

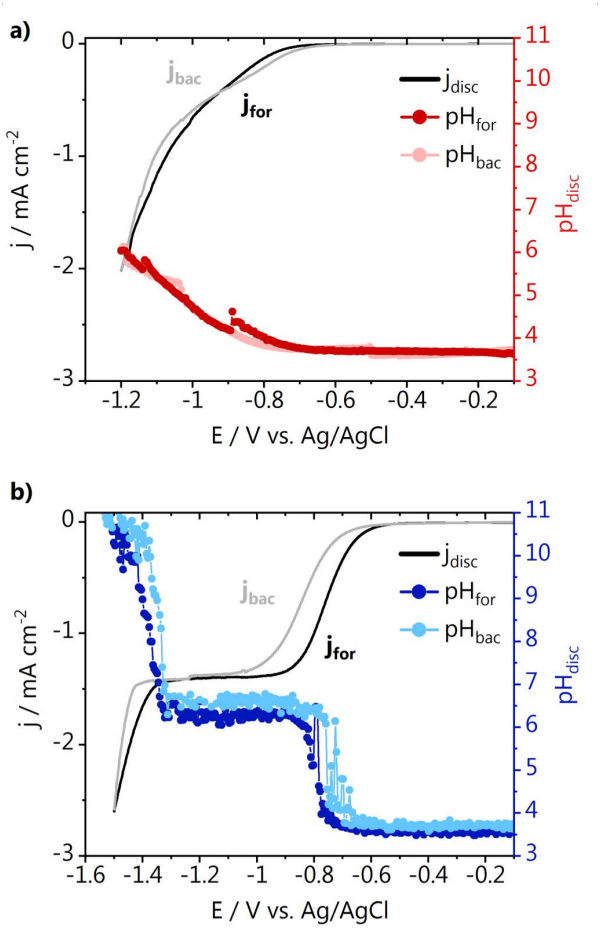

Fig. 6.2. Interfacial pH measurement during the disc cyclic voltammetry in 0.1 M argon saturated at 2000 rpm in **a)** KH_2PO_4 pH_{bulk} = 3.7 and **b)** K_2SO_4 pH_{bulk} = 3.5. CVs were recorded at 2 mV s^{-1} and the 4-HATP/4-NSTP CVs at 200 mV s^{-1}. The forward and backward scans are indicated as j_{for}, pH_{for} and j_{bac}, pH_{bac}.

buffer. For sulphate, the analytical description of Yokoyama et al.[22] is used (Eq. C2 in Appendix C). In the case of phosphate, we have added a correction to account for the homogeneous reactions involving the different phosphate species ($H_2PO_4^-$, HPO_4^-, PO_4^-) that take place upon increase in the local alkalinity (see Eq. C.7-C.29 in the section C.2 "Calculation of the interfacial disc pH" in Appendix C). In Fig. 6.2, we observe that the pH profiles are nearly a mirror image of the current density in both phosphate and sulphate electrolytes. In Fig. 6.2a, we see a gradual increase in current and interfacial pH from 0 to –0.9 V vs. Ag/AgCl. At more negative potentials there is steeper increase in current, likely due to the transition from proton reduction to water and biphosphate reduction as the main branch of HER taking place.[34] Despite the high current, the interfacial disc pH does not go above 6, due to the buffer capacity of the phosphate electrolyte used. In sulphate electrolyte (Fig. 6.2b) a more well-defined plateau is present due to diffusion limited proton reduction ($2H^+ + 2e^- \rightarrow H_2$) followed by a steep increase in current due to water reduction ($2H_2O + 2e^- \rightarrow H_2 + 2OH^-$). The activity for proton reduction starts to increase at about –0.55 V vs. Ag/AgCl and a consequent increase in the interfacial disc pH starts to be observed from –0.57 V vs. Ag/AgCl onwards. This slight delay of 20 mV in the pH response in comparison to the current response is likely because at the very low overpotentials the reaction is only limited by the rate of charge transfer at the electrode-solution interface and there are no pronounced changes in the local proton concentration. At potentials more negative than –0.57 V vs. Ag/AgCl a combination of charge and mass transfer processes control the reaction, and the interfacial pH starts increasing. In the potential window in which the diffusion limited proton reduction plateau is observed, the interfacial disc pH remains around 6.5, until the activity for water reduction increases and consequently the interfacial pH gradually becomes more alkaline. The differences in activity between phosphate and sulphate electrolyte are likely due to the fact that it has been shown that phosphate can outcompete water as a proton donor for hydrogen evolution.[34] We see that due to the high time resolution achieved with the 4-HATP/4-NSTP sensor in combination with the low scan rate of the CV (2 mV s^{-1}), detailed information regarding the correlation between current and pH can be obtained. In principle, the disc voltammetry can also be recorded at higher scan rates, at the expense of the resolution of the pH measurement.

Next, we have performed pH measurements while applying different potentials to the disc electrode. In between potential steps, HER was turned “off”

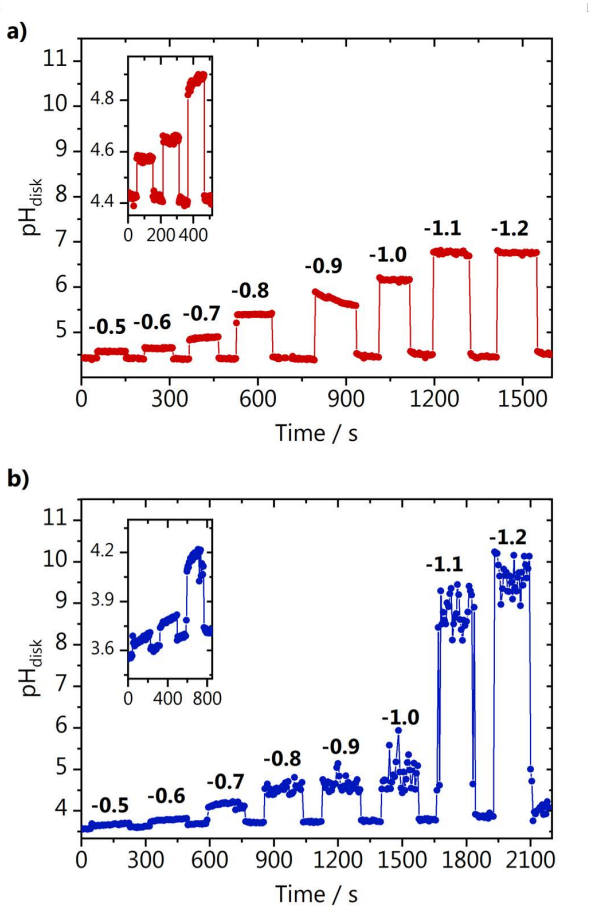

Fig. 6.3. Interfacial pH measurement during chronoamperometry (potentials indicated in the graph in V vs. Ag/AgCl) in 0.1 M argon saturated **a)** KH_2PO_4 pH_{bulk} = 4.4 and **b)** K_2SO_4 pH_{bulk} = 3.6 at 1600 rpm.

by applying 0 V vs. Ag/AgCl to the disc and the ring voltammetry was constantly recorded. The current and potential recorded in time can be seen in Fig. C.4 in Appendix C. Results are shown in Fig. 6.3 for HER carried out in phosphate and sulphate electrolyte. The increase in interfacial pH as a function of potential here is slightly larger than what was observed for the cyclic voltammetry from Fig. 6.2. This is due to the lower rotation rate (1600 rpm) employed during the chronoamperometry, slowing down the transport of species away from the electrode surface. At the low overpotentials, we can accurately detect differences in

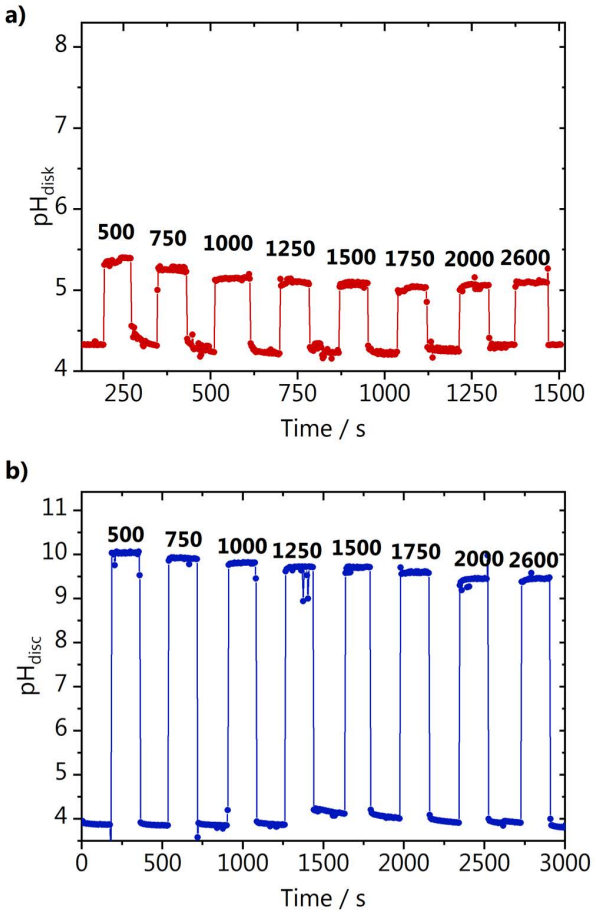

Fig. 6.4. Interfacial pH measurements during chronopotentiometry (constant current density = –0.42 mA cm^{-2}) in 0.1 M argon saturated **a)** KH_2PO_4 pH_{bulk} = 4.4 and **b)** K_2SO_4 pH_{bulk} = 4.0 at the different rotations indicated in the graph in rpm.

interfacial pH as small as 0.1 pH unit, which has not been previously reported for RRDE pH measurements. This is due to the better sensitivity of the 4-HATP/4-NSTP redox couple used in this work compared to the commonly used pH sensors. The insets in Fig. 6.3a and Fig. 6.3b show the pH measured at –0.5, –0.6 and –0.7 V vs. Ag/AgCl, and highlight how the interfacial pH in the phosphate electrolyte always returns to the bulk pH value once the reaction is turned "off". The same does not happen in sulphate, where the baseline keeps increasing due to the lower buffer capacity of the electrolyte. The phosphate electrolyte has different strong buffering regions, namely at pH values around the pK_a of the following reversible reactions:

$H_3PO_4 \rightleftharpoons H_2PO_4^-$ (pK_a = 2.3), $H_2PO_4^- \rightleftharpoons HPO_4^{2-}$ (pK_a = 7.2) and $H_2PO_4^- \rightleftharpoons PO_4^{3-}$ (pK_a = 12.1). In contrast, in the sulfate electrolyte, only one equilibrium reaction is present ($HSO_4^- \rightleftharpoons SO_4^{2-}$) with pK_a = 1.8, considerably lower than the pH developed during HER. It is important to point out that fluctuations of the pH response as observed, for example, at large overpotentials in Fig. 6.3b, occur due to bubbles accumulating near the ring electrode. Even though in this work this did not compromise the measurements, for more challenging systems (or working conditions) this can be circumvented by coating the spacer that separates the ring and the disc electrodes with dopamine.[35]

The buffer capacity of the electrolyte, the current density, and especially the rotation rate, determine the magnitude of the pH gradients developed during RRDE experiments. Therefore, we have also probed to which extent enhancing mass transport affects the interfacial disc pH by performing chronopotentiometry measurements in the same phosphate and sulphate electrolytes. The reaction was turned "on" and "off" by applying a constant current density of –0.4 mA cm^{-2} or –0.001 mA cm^{-2} to the disc, at different rotation rates (see Fig. C.5 in Appendix C for the current and potential recorded). Fig. 6.4 a shows the interfacial disc pH during HER in phosphate electrolyte at different rotation rates. Although the changes in pH are not drastic, we see that between 500 and 1000 rpm, the convective flow of species is not high enough to avoid a larger increase in the local alkalinity, despite the buffer capacity of the electrolyte. Still, the interfacial pH when HER is "on" decreases by increasing the rotation rate. At rotations higher than 1250 rpm, a steady state is reached, i.e. the highest flux of species outwards is achieved and increasing rotation no longer decreases the local alkalinity. This happens because a maximum efficiency at which species move from the disc to the ring is reached, as also discussed in the work of Zimer et al.[11] Due to the buffering species in the phosphate electrolyte, which have easier access to the surface at the higher rotations, the interfacial disc pH in phosphate equilibrates at values around 5.2 at steady state. A different behaviour is observed in the sulphate electrolyte (Fig. 6.4b). Here, although increasing rotation also gradually decreases the interfacial disc pH, a stable pH is never reached at high rotation rates, due to the low buffer capacity of the electrolyte. Additionally, the interfacial disc pH never returns to the bulk value when the reaction is turned "off" (in between different rotations), similarly to what we observed in the chronoamperometry experiment in sulfate (inset of Fig. 6.3b). It is important to point out that even though the calculated interfacial disc pH changes are relatively large, the differences in E_{peak} recorded at the ring electrode

are rather small. Fig. C.6 in Appendix C exemplifies that with the E_{peak} recorded for the experiments shown in Fig. 6.4. The changes in E_{peak} observed during the whole experiment are in the 15-40 mV range, highlighting once more how important it is to employ a sensitive pH sensor for RRDE pH measurements.

6.4 Discussion

The results shown demonstrate that, even though RRDE systems are used to avoid (or minimize) concentration gradients during electrochemical reactions, the effectiveness of the enhancement in mass transport is highly dependent on the electrolyte buffer capacity and on the currents drawn. Assuming "well-defined mass transport conditions" when working with RRDE does therefore not imply absence of concentration gradients, as we see that (in our working conditions) the interfacial disc pH can vary up to 6-7 pH units from the bulk pH. This has important consequences, for example, for measurements performed as a function of rotation rate going from low to high rotations. The interfacial pH values will be significantly different, and their effect is difficult to deconvolute, unless proper quantification of the pH is carried out. In the electrolytes studied, even with a relatively high buffer capacity (phosphate electrolyte) and rotation rates (> 1250 rpm), the interfacial disc pH differed by 1 unit from the bulk. Operating in the steady state regime (strong buffer, high rotations) minimizes convoluted responses due to differences in the interfacial disc pH. However, as evidenced by our results, this regime is strongly dependent on the electrolyte and reaction activity, and has to be identified for each individual system studied. Using the 4-HATP/4-NSTP redox couple as pH sensor on the ring electrode, allows to do so with high temporal resolution and sensitivity. The synthesis of the functionalized gold ring shown in this work is much simpler than what was previously reported for IrO_x[11], highly reproducible, and the system is versatile in terms of disc materials that can be employed, and reactions to be studied.[33] Finally, even though the analytical description from Albery and Calvo[19–21] and Yokoyama et al.[22] is accurate for calculating pH_{disc} for measurements performed in unbuffered electrolytes, here we present a method to correct the description when working in buffered solutions. This is crucial to avoid an overestimation of the interfacial disc pH in buffered systems.

6.5 Conclusions

In this work we have shown that RRDE interfacial pH measurements can be performed with high sensitivity and temporal resolution using a voltammetric pH sensor. A gold ring functionalized with the 4-HATP/4-NSTP redox couple has been used to study pH gradients developing during hydrogen evolution at a gold disc electrode. The interfacial disc pH is measured in phosphate or sulphate electrolyte during different electrochemical experiments: cyclic voltammetry, chronoamperometry and chronopotentiometry. We observed that the changes in interfacial pH at the disc strongly depend on the buffer capacity of the electrolyte and the current drawn (i.e. the activity). By varying the rotation rate at constant current density, we identify the minimum rotation required to achieve the maximum enhancement of mass transport possible and avoid strong concentration gradients during the electrocatalytic measurements. Using HER as a model system, we show that the 4-HATP/4-NSTP voltammetric pH sensor is a powerful tool for accurately measuring interfacial pH with RRDE, with high time resolution.

References

(1) Monteiro, M. C. O.; Koper, M. T. M. *Curr. Opin. Electrochem.* 2021, *25*, 100649.
(2) Goyal, A.; Koper, M. T. M. *Angew. Chemie Int. Ed.* 2021, *60* (24), 13452–13462.
(3) Zhang, Z.; Melo, L.; Jansonius, R. P.; Habibzadeh, F.; Grant, E. R.; Berlinguette, C. P. *ACS Energy Lett.* 2020, *5* (10), 3101–3107.
(4) Giordano, L.; Han, B.; Risch, M.; Hong, W. T.; Rao, R. R.; Stoerzinger, K. A.; Shao-Horn, Y. *Catal. Today* 2016, *262*, 2–10.
(5) Li, M. F.; Liao, L. W.; Yuan, D. F.; Mei, D.; Chen, Y.-X. *Electrochim. Acta* 2013, *110*, 780–789.
(6) Monteiro, M. C. O.; Jacobse, L.; Touzalin, T.; Koper, M. T. M. *Anal. Chem.* 2020, *92* (2), 2237–2243.
(7) Santos, C. S.; Lima, A. S.; Battistel, D.; Daniele, S.; Bertotti, M. *Electroanalysis* 2016, *28* (7), 1441–1447.
(8) Dieckhöfer, S.; Öhl, D.; Junqueira, J. R. C.; Quast, T.; Turek, T.; Schuhmann, W. *Chem. – A Eur. J.* 2021, *27* (19), 5906–5912.
(9) Nadappuram, B. P.; McKelvey, K.; Al Botros, R.; Colburn, A. W.; Unwin, P. R. *Anal. Chem.* 2013, *85* (17), 8070–8074.
(10) Morris, C. A.; Chen, C. C.; Ito, T.; Baker, L. A. *J. Electrochem. Soc.* 2013, *160* (8), H430–H435.
(11) Zimer, A. M.; Medina da Silva, M.; Machado, E. G.; Varela, H.; Mascaro, L. H.; Pereira, E. C. *Anal. Chim. Acta* 2015, *897*, 17–23.
(12) Figueiredo, M. C.; Arán-Ais, R. M.; Climent, V.; Kallio, T.; Feliu, J. M. *ChemElectroChem* 2015, *2* (9), 1254–1258.
(13) Zhang, F.; Co, A. C. *Angew. Chemie - Int. Ed.* 2020, *59* (4), 1674–1681.
(14) Steegstra, P.; Ahlberg, E. *J. Electroanal. Chem.* 2012, *685*, 1–7.
(15) Leenheer, A. J.; Atwater, H. A. *J. Electrochem. Soc.* 2012, *159* (9), H752–H757.
(16) Yang, K.; Kas, R.; Smith, W. A. *J. Am. Chem. Soc.* 2019, *141* (40), 15891–15900.
(17) Ayemoba, O.; Cuesta, A. *ACS Appl. Mater. Interfaces* 2017, *9* (33), 27377–27382.
(18) Henckel, D. A.; Counihan, M. J.; Holmes, H. E.; Chen, X.; Nwabara, U. O.; Verma, S.; Rodríguez-López, J.; Kenis, P. J. A.; Gewirth, A. A. *ACS Catal.* 2021, *11* (1), 255–263.
(19) Albery, W. J.; Calvo, E. J. *J. Chem. Soc. Faraday Trans. 1 Phys. Chem. Condens. Phases* 1983, *79* (11), 2583–2596.
(20) Albery, W. J.; Mount, A. R. *J. Chem. Soc. Faraday Trans. 1 Phys. Chem. Condens. Phases* 1989, *85* (5), 1181.
(21) Albery, W. J.; Mount, A. R. *J. Chem. Soc. Faraday Trans. 1 Phys. Chem. Condens. Phases* 1989, *85* (11), 3717.
(22) Yokoyama, Y.; Miyazaki, K.; Miyahara, Y.; Fukutsuka, T.; Abe, T. *ChemElectroChem* 2019, *6* (18), 4750–4756.
(23) Steegstra, P.; Ahlberg, E. *Electrochim. Acta* 2012, *76*, 26–33.
(24) Bard, A. J.; Mirkin, M. V. Second.; Bard, A. J., Mirkin, M. V., Eds.; CRC Press, 2012.
(25) Chen, X.; McCrum, I. T.; Schwarz, K. A.; Janik, M. J.; Koper, M. T. M. *Angew. Chemie - Int. Ed.* 2017, *56* (47), 15025–15029.
(26) García, G. *ChemElectroChem* 2017, *4* (3), 459–462.
(27) Xue, S.; Garlyyev, B.; Watzele, S.; Liang, Y.; Fichtner, J.; Pohl, M. D.; Bandarenka, A. S. *ChemElectroChem* 2018, *5* (17), 2326–2329.
(28) Rodriguez, P.; Koper, M. T. M. *Phys. Chem. Chem. Phys.* 2014, *16* (27), 13583–13594.

(29) García, G.; Koper, M. T. M. *ChemPhysChem* 2011, *12* (11), 2064–2072.
(30) Kita, H.; Shimazu, K.; Kunimatsu, K. *J. Electroanal. Chem.* 1988, *241* (1–2), 163–179.
(31) Rossmeisl, J.; Chan, K.; Skúlason, E.; Björketun, M. E.; Tripkovic, V. *Catal. Today* 2016, *262*.
(32) Monteiro, M. C. O.; Jacobse, L.; Touzalin, T.; Koper, M. T. M. *Anal. Chem.* 2020, *92* (2), 2237–2243.
(33) Monteiro, M. C. O.; Jacobse, L.; Koper, M. T. M. *J. Phys. Chem. Lett.* 2020, *11* (22), 9708–9713.
(34) Jackson, M. N.; Surendranath, Y. *J. Am. Chem. Soc.* 2016, *138* (9), 3228–3234.
(35) Vos, J. G.; Koper, M. T. M. *J. Electroanal. Chem.* 2019, *850*, 113363.